nature neuroscience

Bilateral olfactory sensory input enhances chemotaxis behavior

Matthieu Louis[1], Thomas Huber[2], Richard Benton[1,3], Thomas P Sakmar[2] & Leslie B Vosshall[1]

Neural comparisons of bilateral sensory inputs are essential for visual depth perception and accurate localization of sounds in space. All animals, from single-cell prokaryotes to humans, orient themselves in response to environmental chemical stimuli, but the contribution of spatial integration of neural activity in olfaction remains unclear. We investigated this problem in *Drosophila melanogaster* larvae. Using high-resolution behavioral analysis, we studied the chemotaxis behavior of larvae with a single functional olfactory neuron on either the left or right side of the head, allowing us to examine unilateral or bilateral olfactory input. We developed new spectroscopic methods to create stable odorant gradients in which odor concentrations were experimentally measured. In these controlled environments, we observed that a single functional neuron provided sufficient information to permit larval chemotaxis. We found additional evidence that the overall accuracy of navigation is enhanced by the increase in the signal-to-noise ratio conferred by bilateral sensory input.

The general principles governing orientation in chemical gradients have long been studied in various organisms, from the bacterium *Escherichia coli* to mammals[1–7]. The signaling pathways involved in directional sensing have been thoroughly investigated in prokaryotic and eukaryotic cells, such as *E. coli*[8], the budding yeast[9] and *Dictyostelium discoideum*[10]. Although most bacteria navigate using indirect random locomotion that is biased in the direction of the chemical gradient, certain unicellular organisms are able to locally extract directional information about the gradient[11]. Mathematical models can explain how signaling networks achieve sensing and amplification of external signals, noise filtering and locomotion[12,13]. These models guided experiments that showed that *Caenorhabditis elegans* navigates toward chemical attractants according to an improved random-walk strategy[14].

Chemotaxis involves direct navigation toward attractive chemicals and away from aversive chemicals. In contrast with the indirect biased random-walk strategies adopted by *E. coli*, this process requires computing odorant gradients locally and directing motion along, or against, the direction of steepest concentration change. The gaseous nature of the atmosphere in which most insects and mammals evolved makes this detection problem potentially more complicated than in liquid phase. It may therefore require sophisticated data integration that is supported by the processing capacity of neuronal networks. How brains solve this problem is an important, but understudied, question.

Addressing this question is difficult, as the stimulus space of olfaction is unique among the senses in its diversity and discontinuity. Tens of thousands of odor molecules, which differ in size, polarity, functional group and vapor pressure, are thought to exist. Gaseous odorants interact with odorant receptors in the sensory cilia of olfactory sensory neurons (OSNs), leading to the conscious perception of an odor[15]. Olfactory studies in species from *C. elegans* to humans have relied on a small subset of several dozen odors[16–18]. Yet differences in odor-delivery methods make it essentially impossible to compare stimuli concentrations between different studies. This problem is further exacerbated by the gaseous state of the stimuli, which travel in discontinuous packets that are propelled by turbulence in the environment[19]. There have been few attempts to generate odorant environments with predictable and measurable properties[20,21]. We addressed this problem by developing a new behavioral assay where the quantity and distribution of the olfactory stimulus can be controlled and precisely quantified in space.

Using this assay, we delineated the behavioral and neural mechanisms underlying chemosensory orientation in a genetically manipulatable organism with a simple CNS, the *D. melanogaster* larva. These animals show robust odor-driven responses[22–24] that are controlled by an olfactory system that is anatomically similar to, yet far simpler than, that of vertebrates. The larval olfactory system is composed of 21 pairs of OSNs housed in two bilaterally symmetric dorsal organs at the tip of the head[23]. Each OSN expresses one, or occasionally two, specific odorant receptors together with *Or83b*, a ubiquitously expressed co-receptor[25,26]. The full repertoire of odorant receptor genes expressed in the larva has been characterized by us and others[24,27]. Using genetic and transgenic approaches[24], we manipulated the expression of odorant receptor genes to generate animals with only a single functional OSN on either the left or right side of the head. We used our controlled odorant gradients and animals with unilateral olfactory input to ask whether bilateral input is necessary for odorant-gradient sensing in larvae.

[1]Laboratory of Neurogenetics and Behavior, The Rockefeller University, 1230 York Avenue, New York, New York 10065, USA. [2]Laboratory of Molecular Biology and Biochemistry, The Rockefeller University, 1230 York Avenue, New York, New York 10065, USA. [3]Present address: Center for Integrative Genomics, Genopode Building, University of Lausanne, CH-1015 Lausanne, Switzerland. Correspondence should be addressed to L.B.V. (leslie@rockefeller.edu).

Received 25 July; accepted 29 November; published online 23 December 2007; doi:10.1038/nn2031

RESULTS

Spectroscopic measurements of odorant gradients

Several dozen odors elicit strong behavioral attraction in *Drosophila* larvae and a few have been shown to induce repellent activity[22,28]. Previously, odor-evoked behaviors were quantified in assays where an odor source was placed at the edge of an agarose-coated Petri dish and the fraction of animals accumulating on the odor side of the plate was quantified over a fixed period of time[22,24,28]. Although these assays have provided useful information about the ability of larvae to respond to various odors, they failed to reveal any information about the mechanisms governing orientation in chemical gradients. Addressing this problem requires local measurements of odorant concentrations and the shape of the odorant-gradient field. We took physical measurements of odor concentrations in vapor phase to determine the mechanism by which *Drosophila* larvae ascend the trail of attractive odors.

To obtain environments with odorant gradients of defined spatial properties, we devised two odorant-gradient devices (**Fig. 1** and **Supplementary Fig. 1** online). The single–odor-source device (**Fig. 1a**,**c**,**e**) was designed with a radially symmetric odorant gradient emanating from a point source near the center of the behavioral arena. The multiple–odor-source device generates a gradient centered along the length of the plate with a shape and amplitude controlled by the concentrations of the odor sources (**Fig. 1b**,**d**,**f**). To verify the existence of odorant gradients in these devices, we exploited the characteristic infrared absorption spectra of odorant molecules to measure their concentration in vapor phase and characterize their geometries (**Supplementary Figs. 2–7** online).

The single–odor-source device was constructed using the lid of a standard 96-well plate (**Fig. 1a**). The condensation ring at position E7 was filled with 10 µl of a given odor diluted in paraffin oil. Here we used isoamyl acetate, an ester abundant in ripe banana. The lid containing the odor droplet was then inverted above a surface of agarose to create a closed space. Using Fourier transform–infrared (FT-IR) spectroscopy, we computed the absorbance of infrared light through air along the length of the single–odor-source device (**Fig. 1c** and **Supplementary Fig. 2**). The average concentration of odor along this line was calculated by using the Beer-Lambert law. The molar extinction coefficient of the odor was determined in gaseous phase (**Supplementary Fig. 3**). Lowering the source concentration by half reduced the overall amplitude of the resulting gradient by a factor of two (**Fig. 1c**). On free diffusion of the odor from the centered source, the odor had a Gaussian profile that was stable for several minutes (**Fig. 1c**). By fitting numerical simulations with the infrared concentration profile (**Fig. 1c** and **Supplementary Methods** online), we estimated the absolute odor concentration at every point of the gradient (**Fig. 1e**).

The multiple–odor-source device was constructed by filling every other condensation ring along row E in the lid of a 96-well plate with decreasing concentrations of 10 µl of odor diluted in paraffin oil (**Fig. 1b**). Odor concentrations were computed with infrared spectroscopy along the length and width of the plate (**Supplementary Fig. 2**) once every minute (**Supplementary Fig. 4**). For a series of six sources with concentrations ranging between 0.03–1.00 M (**Fig. 1b**), the resulting two-dimensional odorant gradient peaked under the odorant line and increased exponentially along the length (**Fig. 1d**). The geometry of the gradient field can be varied independently from its amplitude by fixing the absolute concentrations of odor in each source separately. Notably, the shape of the gradient field is stable for at least 15 min, is reproducible between independent trials (**Supplementary Fig. 5**) and is only minimally perturbed by manipulations necessary to introduce animals onto the plate (**Supplementary Fig. 5**). On the basis of the one-dimensional length and width profiles (**Fig. 1d**), we reconstructed the topography of the gradient field (**Fig. 1f** and **Supplementary Fig. 7**).

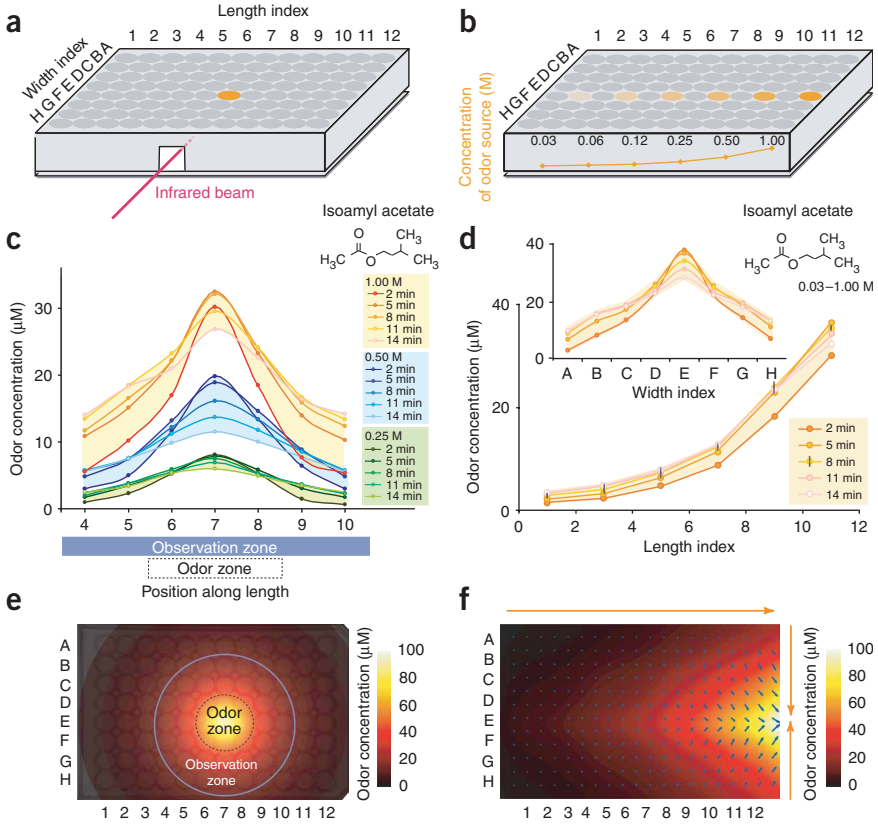

Figure 1 FT-IR spectroscopy used to measure odorant gradients in single and multiple source odor devices. (**a**) Schematic of the single–odor-source device. (**b**) Schematic of the multiple–odor-source device. The loading concentration (M) of odor droplets placed along row E follows a binary dilution series ranging between 0.03 and 1.00 M. (**c**) Time course of the cumulative odor concentrations in gaseous phase (in µM) obtained at fixed positions along the length of the single–odor-source device. Profiles are color coded according to the concentration of the odor source (red, 1.00 M; blue, 0.50 M; green, 0.25 M). The observation zone corresponds to the largest circular area excluding any walls of the plate (diameter, 3.5 cm). The odor zone is a smaller circular area centered on the odor source in the observation zone (diameter, 1.4 cm). (**d**) Concentration profiles (µM) of the odor in gaseous phase obtained by infrared spectroscopy along the length and width (inset) of the multiple–odor-source device. The concentrations reported are the means of three independent measurements (**Supplementary Fig. 5**) and s.d. are represented as black error bars for time $t = 8$ min. (**e**) Simulated single–odor-source gradient extrapolated from infrared absorbance measurements (see **Supplementary Methods** and **Supplementary Fig. 6**). (**f**) Topographic reconstruction of the multiple–odor-source gradient, based on infrared absorbance measurements averaged over 4–12 min (see **Supplementary Methods**).

Chemotaxis behavior in gradients of defined shape

The navigation ability of *Drosophila* larvae was characterized in these stable and defined odorant gradients. Individual animals were first monitored in the single–odor-source device after their introduction near the odor source (**Fig. 2**). To quantify the degree of attraction of a given stimulus, we computed the percentage of time spent by each larva

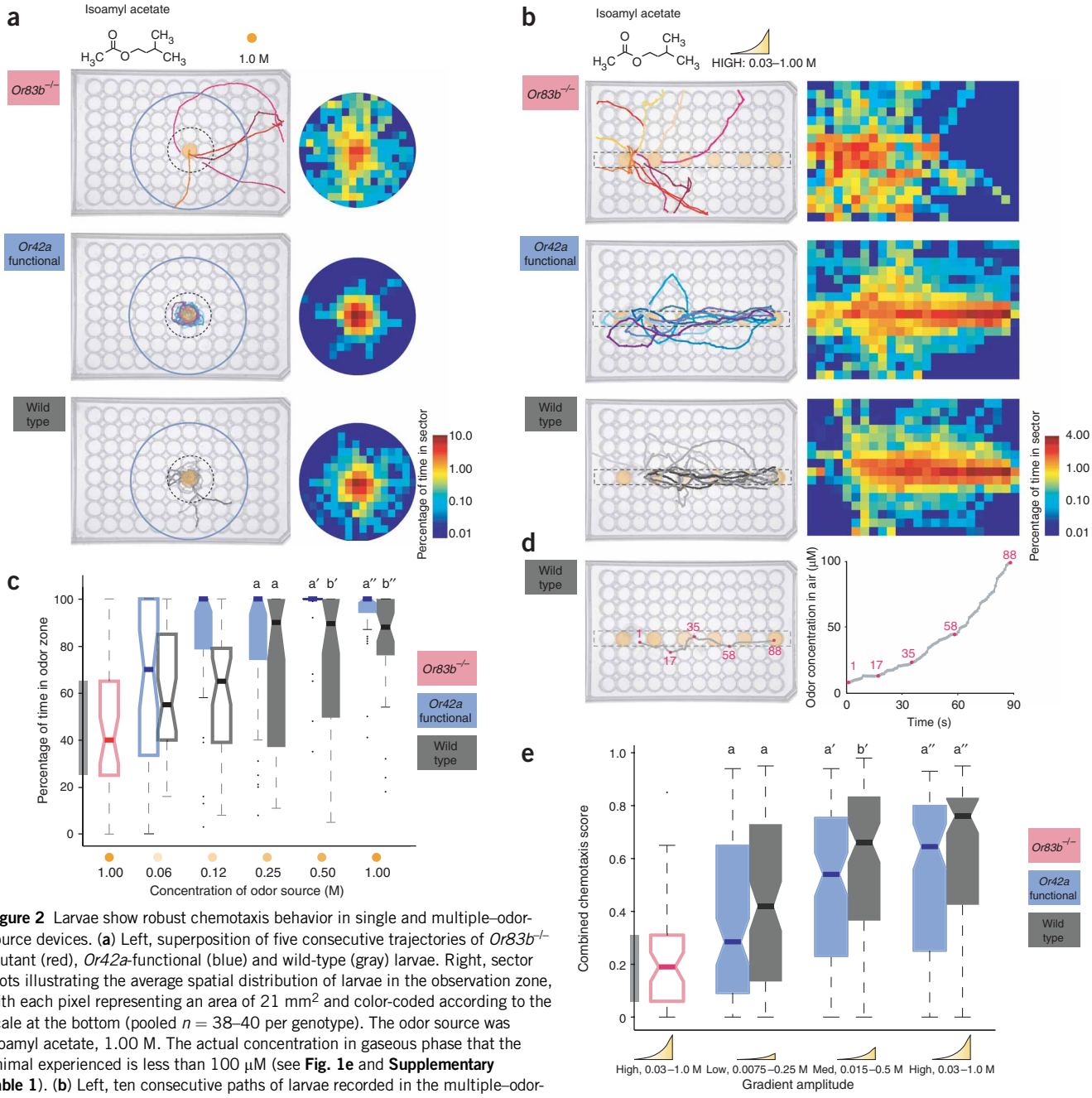

Figure 2 Larvae show robust chemotaxis behavior in single and multiple–odor-source devices. (**a**) Left, superposition of five consecutive trajectories of *Or83b*$^{-/-}$ mutant (red), *Or42a*-functional (blue) and wild-type (gray) larvae. Right, sector plots illustrating the average spatial distribution of larvae in the observation zone, with each pixel representing an area of 21 mm^2 and color-coded according to the scale at the bottom (pooled $n = 38$–40 per genotype). The odor source was isoamyl acetate, 1.00 M. The actual concentration in gaseous phase that the animal experienced is less than 100 μM (see **Fig. 1e** and **Supplementary Table 1**). (**b**) Left, ten consecutive paths of larvae recorded in the multiple–odor-source device. Right, sector plots of the average spatial distribution of larvae color-coded according to the scale at the bottom. Sector plots represent pooled data from all animals examined (*Or83b*$^{-/-}$, $n = 50$; *Or42a* functional and wild type, $n = 100$). The odor source was a high-amplitude exponential gradient of isoamyl acetate, 0.03–1.00 M. The actual concentration in gaseous phase that the animal experienced is less than 100 μM (see **Fig. 1f**). (**c**) Percentage of time spent by individual animals in the odor zone of the single–odor-source device. (**d**) Left, representative trajectory of a wild-type animal navigating in a high-amplitude exponential gradient, with five time points (s) indicated in magenta. Right, plot of absolute odor concentration in gaseous phase versus time of the animal at left. (**e**) Dose dependence of larval chemotaxis measured for multiple–odor-source gradients with increasing amplitudes (low to high), and quantified by a chemotaxis score measuring the average alignment of a trajectory with the odorant line (see Methods). For panels **c** and **e**, boundaries of box plots represent first and third quartiles, whereas the 'waist' indicates the median. Whiskers are 1.5 interquartile distance and outliers are marked with black dots. The gray bar on the *y* axis indicates the interquartile range of the *Or83b*$^{-/-}$ mutant. Samples were individually compared with the *Or83b*$^{-/-}$ control using Wilcoxon tests with a Bonferroni adjustment to maintain the confidence level to 5%. By convention, throughout the paper, we represent samples with a median significantly different from *Or83b*$^{-/-}$ by shaded boxes (Bonferroni corrected, $P < 0.005$ in **c** and $P < 0.0083$ in **e**). Wild type and *Or42a* functional were compared only when both differed significantly from the *Or83b*$^{-/-}$. Box plot bars labeled with different letters are statistically different. Significance was assessed by Wilcoxon test (corrected, $P < 0.0167$ in **c** and **e**).

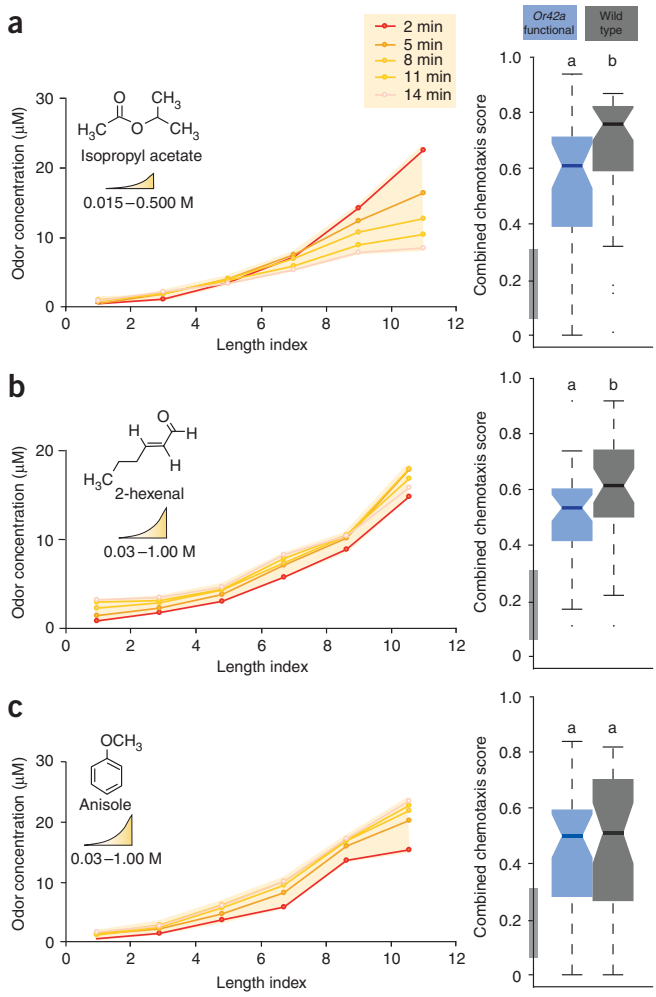

Figure 3 The spectroscopic method for measuring odorant gradients can be generalized to other odors. (**a**) Length profile of the ester isopropyl acetate. (**b**) Length profile of the aromatic compound anisole. (**c**) Length profile of the aldehyde (*E*)-2-hexenal. For each odor, the chemotaxis performance of wild-type and *Or42a*-functional larvae is represented in the graph at the right. Statistical analysis and data presentation are as described in **Figure 2**. For each odor, significance of differences between $Or83b^{-/-}$ measured for isoamyl acetate high exponential gradients, and either wild type or *Or42a* functional was assessed by Wilcoxon test with Bonferroni correction (corrected $P < 0.025$). Differences between wild type and *Or42a* functional were assessed by Wilcoxon test ($P < 0.05$).

in the odor zone (defined in **Fig. 1c**). We tested *Or83b*-null mutant larvae, which were previously shown to lack all odor-evoked behaviors[24,26], and wild-type larvae with 21 pairs of functional OSNs. As previously demonstrated, *Or83b* larvae did not respond to even the highest concentration of isoamyl acetate tested (**Fig. 2a,c**). At low source concentrations (0.06 and 0.12 M), the behavior of wild-type and $Or83b^{-/-}$ mutant larvae was not significantly different (Wilcoxon test, $P > 0.02$). For the higher source concentrations (0.50 and 1.00 M), more than half of the wild-type animals spent over 90% of the trial in the odor zone (**Fig. 2c**). On the basis of a previous study[24], we anticipated that larvae with a single functional OSN expressing *Or42a* would detect the presence of the isoamyl acetate for appropriately high source concentrations. Using larvae in which only the two *Or42a*-expressing OSNs on either side of the head were functional, we quantified the degree of attraction for different source concentrations and found that *Or42a*-functional larvae were more sensitive than wild-type animals and that they showed significant responses to source concentrations as low as 0.12 M ($P < 0.005$; **Fig. 2c**).

Having shown that *Or42a*-functional larvae are able to respond to the presence of isoamyl acetate over a range of concentrations that was not smaller than that of wild-type animals, we asked whether the information carried by the *Or42a*-expressing OSNs alone is sufficient to perceive changes in odor concentration and mediate navigation in the multiple–odor-source device (**Fig. 2b,d,e**). Individual animals were introduced at the low-concentration end of the odorant line (position E3–4) and their trajectories were quantitatively characterized (**Supplementary Figs. 8–12** online). $Or83b^{-/-}$ animals dispersed at random, whereas both *Or42a*-functional and wild-type animals efficiently navigated along the odorant line (**Fig. 2b**). A typical wild-type larva covered the total distance of the odorant line in less than 2 min (**Fig. 2d**) and navigated with a constant speed of 0.1 cm s^{-1} throughout the arena (**Supplementary Fig. 8**). The overall alignment of sets of paths with the odorant line was measured by computing a combined chemotaxis score ranging between 0 (complete disregard of the odorant line) and 1 (perfect alignment with the odorant line) (**Supplementary Methods**). The chemotaxis scores of wild-type and *Or42a*-functional larvae were correlated with the amplitude of the gradient and did not differ between the genotypes for two of the three gradient amplitudes that we tested (**Fig. 2e**).

For $Or83b^{-/-}$, wild-type and *Or42a*-functional larvae, we found that the turning rate was inversely correlated with the speed of the animal (**Supplementary Fig. 8**). This trend suggests that larvae slow down while they undergo sharp directional changes, irrespective of their ability to detect the presence of an odorant stimulus. We found no evidence supporting a mechanism suppressing motion as a function of the odor concentration. Instead, we observed that individuals localized and stayed in the neighborhood of the single odor source by continuously turning around it (**Supplementary Fig. 9**).

Generalization of spectroscopic method to other odors

To establish the generality of our spectroscopic method, we tested three other odorants, in the multiple–odor-source device, for both the spectroscopic measurement of odorant gradient and the ability of larvae to chemotax in such environments (**Fig. 3**). Stable exponential gradients were created and measured with infrared spectroscopy for a second ester, isopropyl acetate (**Fig. 3a**), an aromatic compound, anisole (**Fig. 3b**), and an aldehyde, (*E*)-2-hexenal (**Fig. 3c**). Both wild-type and *Or42a*-functional larvae navigated robustly in all three odorant gradients (**Fig. 3**).

Evidence that larvae detect local odorant gradients

To clarify the direct or indirect nature of the orientation mechanism that we observed, we first analyzed the turning rate as a function of the absolute concentration $C(x,y)$ measured for a high-amplitude exponential gradient. The gradient range was subdivided into five concentration zones for which the mean turning rates were calculated (**Fig. 4a**, bottom). On average, wild-type and *Or42a*-functional larvae showed a small tendency to decrease their turning rate as the odor concentration increased (**Fig. 4a** and **Supplementary Fig. 10**). In contrast, this trend was not observed for $Or83b^{-/-}$. Next, we investigated whether larvae are able to orient their motion directly toward the direction of largest concentration increases by locally computing the heading angle between the direction of the odorant gradient (vector field, **Fig. 1f**) and the direction of instantaneous motion at every point of a path (**Supplementary Methods**). If there is a direct orientation mechanism, we expected to find an improvement of the alignment

with the gradient as both the concentration and gradient magnitude increase. We quantified the alignment with the gradient by computing the cosine of the heading angles. Heading angles belonging to the same concentration zone were pooled and the mean of their cosine was determined (**Fig. 4b**). We observed that the local alignment of the direction of motion with the odorant gradient improved as the concentration increased. A similar conclusion was reached when considering the local heading as a function of the gradient magnitude $|\nabla C(x,y)|$ (**Fig. 4c**).

Finally, we searched for additional evidence that would support the hypothesis that *Drosophila* larvae use a direct navigation strategy with alignment on the stimulus and not an indirect biased random walk, which bacteria use. To discriminate between these two strategies, we applied a statistical procedure based on the detection of biases in the

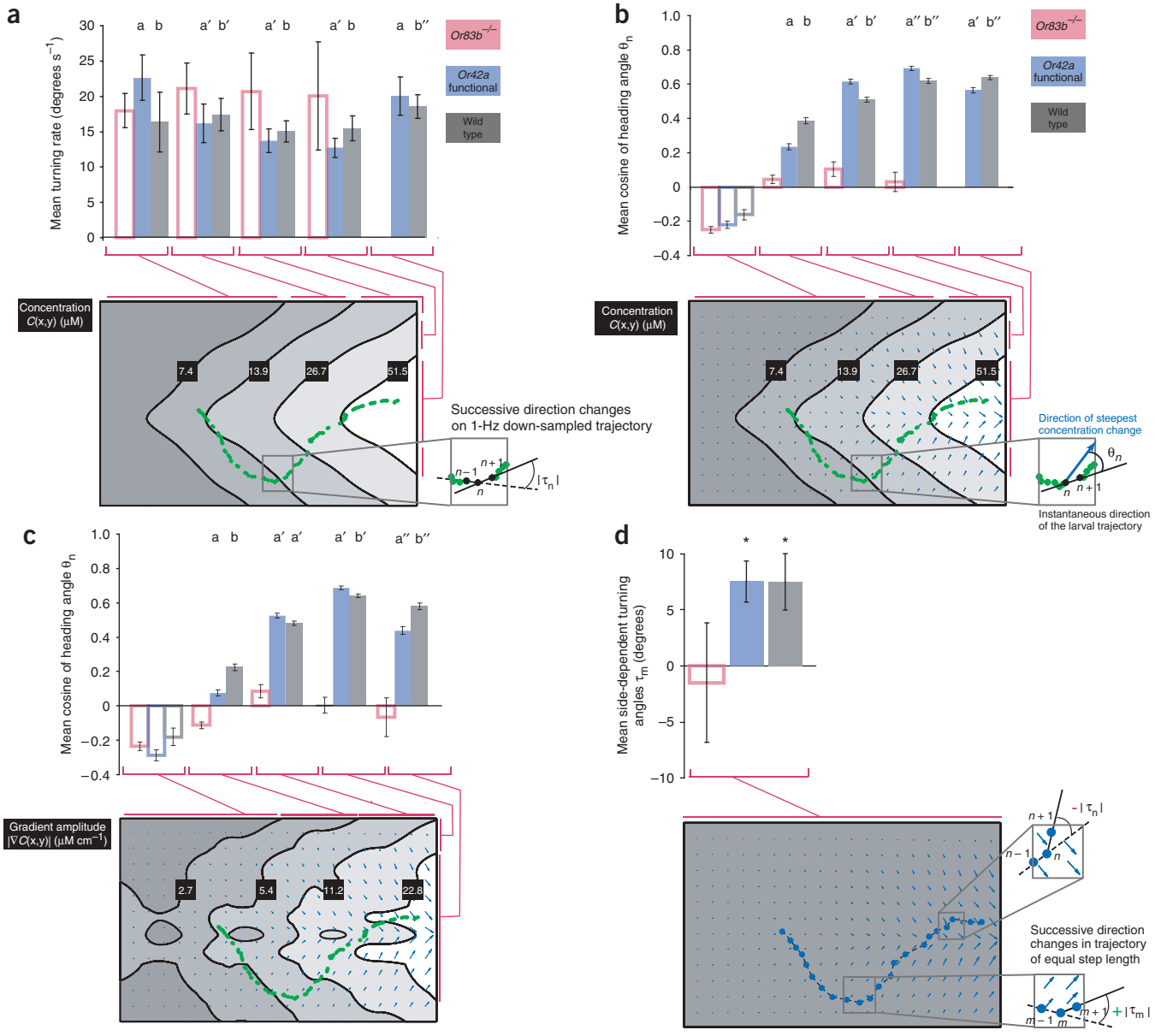

Figure 4 Local heading and turning bias analysis suggests that *Drosophila* larvae are able to detect the direction of local odorant gradients. (**a**) Averaged turning rate as a function of the absolute odor concentration $C(x,y)$ (top). The mean turning rates and 99% confidence interval on distributions corresponding to different concentration zones (bottom) are represented for the three genotypes tested in a high exponential gradient of isoamyl acetate (*Or83b*$^{-/-}$, $n = 50$; *Or42a* functional and wild type, $n = 100$). Turning-rate distributions were compared between concentration zones using the Watson-Wheeler test[47]. The significance of comparisons was assessed with a Bonferroni correction (corrected, $P < 0.005$). (**b**) Averaged cosine of heading angles as a function of the absolute odor concentration. The mean and s.d. of different distributions are presented as in **a**. Mean cosines were compared between concentration zones using *t*-tests. The significance of comparisons with *Or83b*$^{-/-}$ mutant and between wild-type and *Or42a*-functional larvae was assessed with a Bonferroni correction (corrected $P < 0.005$ and $P < 0.0031$, respectively). (**c**) Cosine of heading angles as a function of the gradient magnitude ($|\nabla C(x,y)|$). Statistical significance represented as in **a**. (**d**) Turning-bias analysis of the trajectories of *Or83b*$^{-/-}$ mutant, *Or42a*-functional and wild-type larvae tested in the same conditions as **a**. The analysis was carried out on paths down-sampled to have equal step length. The mean turning angles were calculated with 99% confidence interval. * indicates genotypes that have a nonzero turning-angle distribution[47].

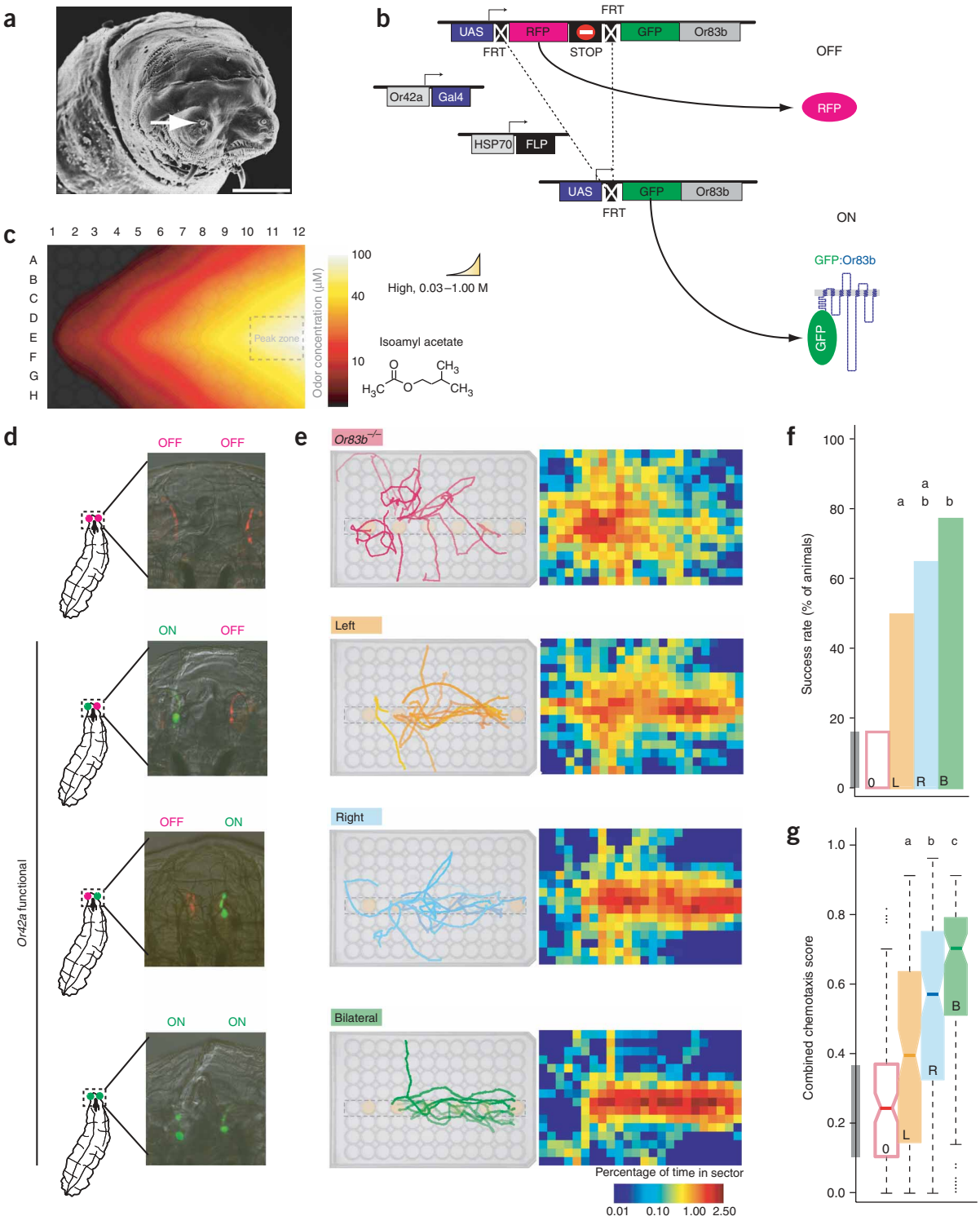

Figure 5 Chemotaxis mediated by a single functional *Or42a* olfactory neuron. (**a**) Scanning electron micrograph of the head of a *Drosophila* larva. The dorsal organs (white arrow) are separated by approximately 100 μm (white scale bar, reproduced from ref. 23). (**b**) Genetic strategy used to generate animals carrying a unilateral rescue of *Or83b*$^{-/-}$ in a single *Or42a*-expressing OSN. (**c**) Reconstructed high-amplitude isoamyl acetate exponential gradient that is color-coded according to the scale at the right. Trajectories reaching the gray box labeled peak zone at the peak of the gradient were considered to be successful. (**d**) Top to bottom, flattened confocal *z*-stack images of the anterior tips of no rescue (0), unilateral left rescue (L), unilateral right rescue (R) and bilateral rescue larvae (B). (**e**) Left, ten consecutive trajectories of same animals as in **d**. Right, sector plots of 100 trajectories from these larvae. (**f**) Percentage of animals reaching the peak zone of the gradient (success rate). For the three comparisons with *Or83b*$^{-/-}$ mutants and those three between rescue phenotypes, the significance of differences between success rates was assessed by Haber's χ^2 test with a Bonferroni correction (corrected $P < 0.0167$). (**g**) Chemotaxis score analysis. Significance of the differences with *Or83b*$^{-/-}$ mutants and between rescue phenotypes was reported using the Wilcoxon test with a Bonferroni correction for three comparisons (corrected $P < 0.0167$). Statistical analysis and data presentation are as described in **Figure 2** ($n = 100$ for all genotypes).

distribution of side-dependent turning angles[29] (**Supplementary Methods** and **Supplementary Fig. 13** online). If larvae implement a direct navigation (taxis[6]), their turns would be preferentially directed toward the gradient and thus show a mean side-dependent turning–angle distribution significantly different from 0. If larvae instead use an indirect biased random walk where, for instance, the turning rate is determined by variations in stimulus intensity, the direction of their turns would be uncorrelated with the stimulus and should lead to a side-dependent turning–angle distribution centered around 0. We found that wild-type larvae showed a turning bias significantly larger than 0 ($P < 0.01$), a characteristic signature of a direct navigation mechanism (**Fig. 4d**). In control experiments, we showed that *Or83b*$^{-/-}$ mutants had no turning bias (**Fig. 4d**). Consistent with this analysis, we found that wild-type and *Or42a*-functional larvae directed more than 63% of the turns toward the gradient, whereas *Or83b*$^{-/-}$ mutant directed turns toward and away from the peak of the gradient with equal probability (49% versus 51%). We conclude that *Drosophila* larvae use a direct chemotaxis mechanism to compute local odorant gradients and move toward the rising concentrations of the odorant gradient.

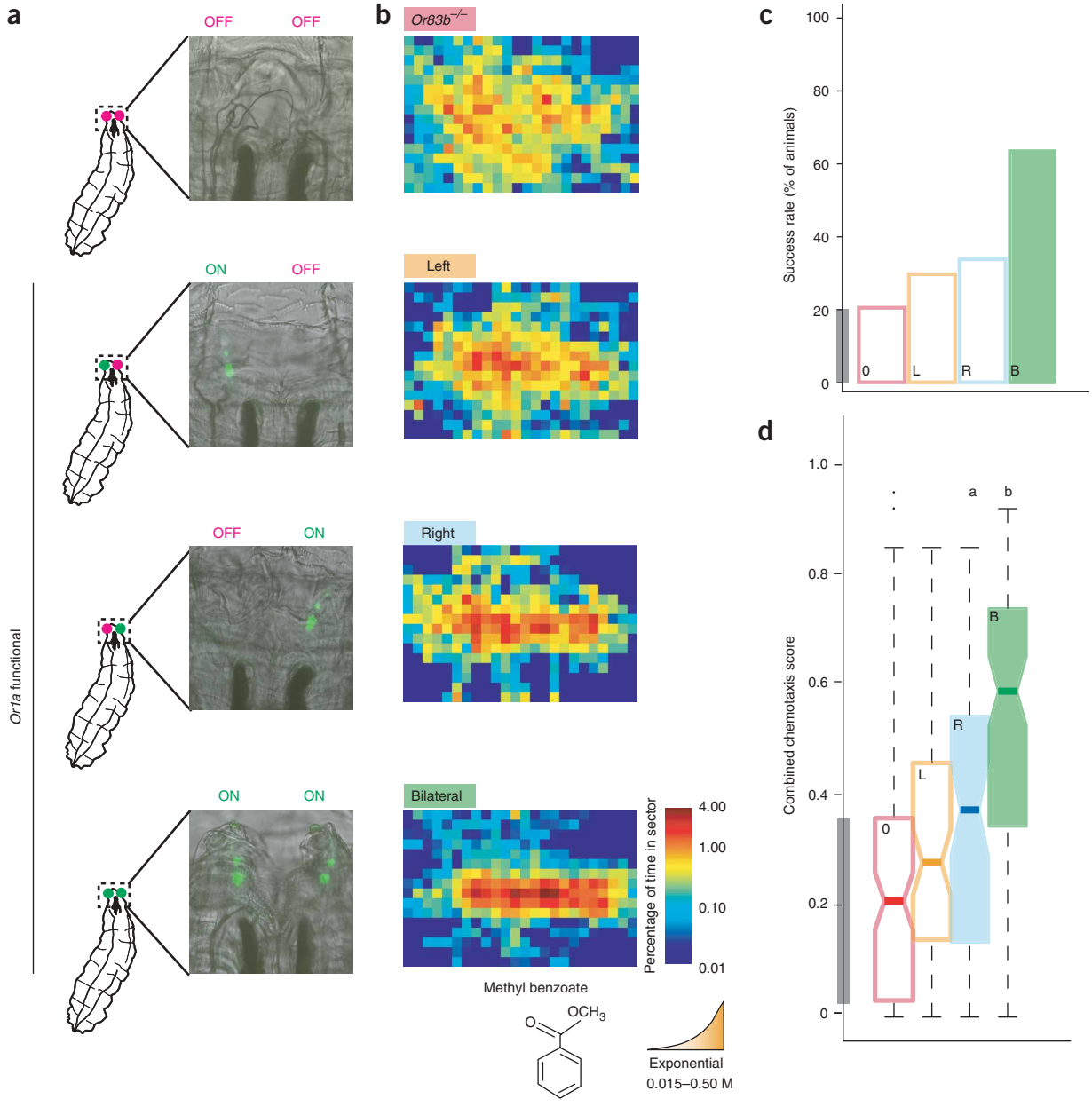

Figure 6 Chemotaxis mediated by a single functional *Or1a* olfactory neuron. (**a**) Top to bottom, flattened confocal *z*-stack images of the anterior tips of no rescue, unilateral left rescue, unilateral right rescue and bilateral rescue larvae. (**b**) Sector plots of 100 trajectories from these larvae. (**c**,**d**) Statistical analysis of success rate (**c**) and chemotaxis score (**d**). After Bonferroni adjustment for three comparisons, differences with *Or83b*$^{-/-}$ mutant were considered significant for corrected $P < 0.0167$. The performances of right and bilateral rescues were significantly different ($P < 0.05$). The odor source was a gradient of methyl benzoate with exponential shape along the plate length, 0.015–0.50 M. Statistical analysis and data presentation are as described in **Figure 2** (*Or83b*$^{-/-}$, $n = 100$; left, $n = 70$; right, $n = 60$; bilateral, $n = 100$).

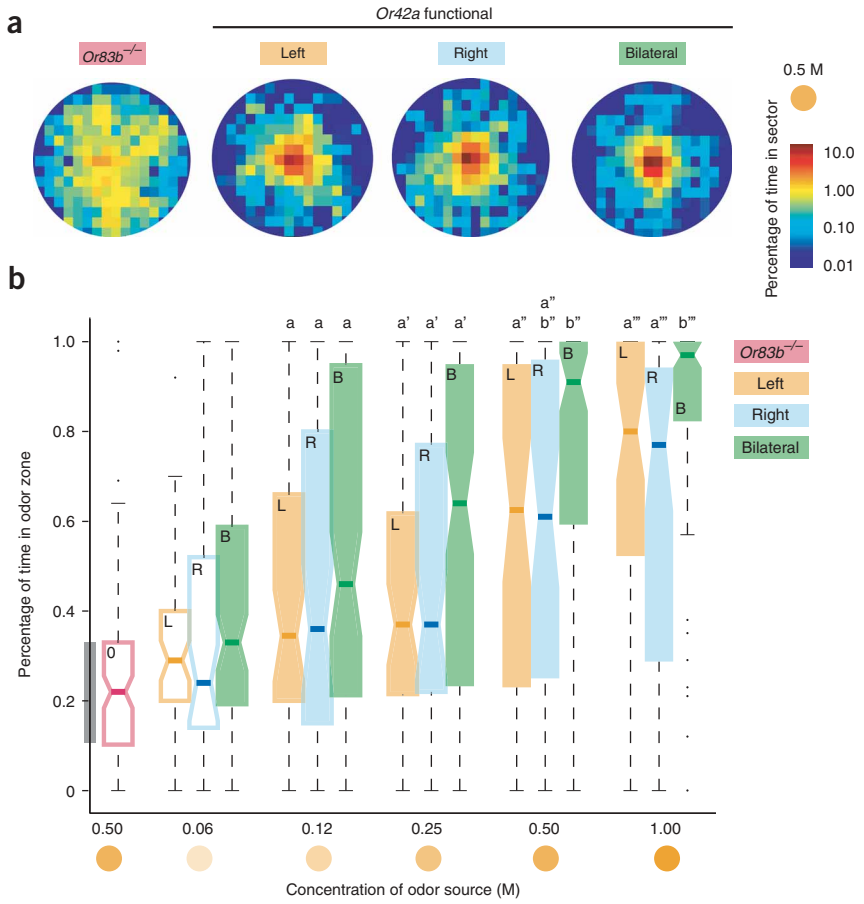

Figure 7 Sensitivity of animals with unilateral or bilateral olfactory function. (**a**) Sector plots of larvae tested with single–odor-source device. The odor source was isoamyl acetate, 0.50 M. (**b**) Dose dependence of larval response measured as the percentage of time spent in the odor zone. Using Wilcoxon test with a Bonferroni correction for 15 comparisons, differences between individual samples and *Or83b*$^{-/-}$ mutant were considered significant for corrected $P < 0.0033$. Samples obtained for the same concentration and differing significantly from *Or83b*$^{-/-}$ mutant were first compared with Kruskal-Wallis tests adjusted for four comparisons (corrected $P < 0.012$). *Post hoc* pair-wise Wilcoxon tests were then applied to compare individual samples corresponding to the same source concentration (corrected $P < 0.0042$). Statistical analysis and data presentation are as described in **Figure 2** (*Or83b*$^{-/-}$, $n = 100$; left, $n = 50$; right, $n = 50$; bilateral, $n = 100$).

performed better than either of the unilateral rescues ($P < 0.0167$; **Fig. 5g**). We found no evidence to support a turning bias in direction of the functional side of the head (**Supplementary Fig. 14** online). To exclude the possibility that right rescues were favored by an asymmetry in the gradient field, we set up high-amplitude exponential gradients along row D instead of along row E. In these conditions, left rescues were not found to behave better than right rescues (**Supplementary Fig. 15** online).

Chemotaxis of the unilateral *Or42a*-functional animals

Drosophila larvae have two symmetric dorsal organs or 'noses', one on each side of the head (**Fig. 5a**). Larval OSNs project strictly ipsilaterally into the larval antennal lobe, in contrast to the largely bilaterally projecting adult olfactory system[24]. Given that the dorsal organs are separated by ~100 μm, we estimate that there is an internasal concentration difference of approximately 10 nM in a gradient with high amplitude and exponential shape. A pair of functional *Or42a*-expressing OSNs, one in each dorsal organ, conveys enough information to permit chemotaxis (**Fig. 2**). To test whether the minute concentration differences between the two dorsal organs could be detected by the larval olfactory system and used to define the local direction of odorant gradients, we generated transgenic animals in which we rescued *Or83b* expression in either the left or right *Or42a*-expressing OSN (**Fig. 5b**).

Animals were tested in multi-source odorant gradients with a high-exponential shape (**Fig. 5c**). The functional state of the *Or42a* OSNs in each larva was scored by confocal analysis after behavioral analysis, with the presence of green fluorescent protein (GFP) fused to Or83b (GFP;Or83b) fluorescence indicating a functional OSN (**Fig. 5d**). Unilaterally rescued larvae were able to ascend exponential gradients, although their paths meandered more than those of bilaterally rescued larvae (**Fig. 5e**). Analysis of the percentage of animals reaching the peak zone of the gradient and the chemo taxis score confirmed this observation (**Fig. 5f**). Animals with a right-functional *Or42a* OSN chemotaxed significantly better than the corresponding left-functional animals, and bilateral rescues

Chemotaxis of the unilateral *Or1a*-functional animals

To confirm the general principles observed with animals possessing one left, one right or two functional *Or42a*-expressing neurons, we generated unilateral and bilateral rescues for the *Or1a* OSN using the scheme above (**Fig. 5b**) with an *Or1a-Gal4* driver (**Fig. 6a**,**b**). *Or1a* OSN is narrowly tuned[24] and selectively activated by methyl benzoate (K. Asahina, unpublished data). Although animals with either a left or right functional *Or1a*-expressing neuron chemotaxed poorly, bilateral rescue larvae detected the methyl benzoate odorant gradient with sufficient accuracy to reach the peak zone of the gradient field in 60% of the trials (**Fig. 6c**). In comparison, 75% of the *Or42a* bilateral rescues reached the peak zone for isoamyl acetate. The limited chemotaxis ability of *Or1a* rescue may explain why no significant attraction to methyl benzoate was found in earlier work[24]. Analysis of the chemotaxis scores revealed that left-functional animals did not behave significantly better than *Or83b*$^{-/-}$ larvae. In contrast, right-functional animals and bilateral rescues chemotaxed significantly better than *Or83b*$^{-/-}$ larvae (**Fig. 6d**). Bilateral rescues performed significantly better than unilateral right rescues (Wilcoxon test, $P < 2 \times 10^{-5}$). These results confirm our previous observations for unilateral rescue of the *Or42a* OSN.

Odor sensitivity of unilateral and bilateral larvae

To exclude the possibility that differences in chemotaxis ability between unilateral and bilateral rescues were a trivial effect of a marked decrease in the sensory thresholds of unilateral larvae, we characterized the lowest odor concentration for which these animals showed significant attraction to isoamyl acetate. Animals were introduced in proximity to

the odor source in the single-source assay. Unilaterally rescued larvae required slightly higher minimal-threshold odor concentrations than the bilaterally rescued larvae to show a significant behavioral response, measured as accumulation near the odor (**Fig. 7**). However, we found no difference between unilateral and bilateral rescues in behavioral responses to higher concentrations of this odorant. On the basis of FT-IR measurements, we estimate that the sensory threshold of unilateral animals to isoamyl acetate is ~10 μM, compared with the ~5 μM threshold in bilateral animals (source concentrations of 0.12 M and 0.06 M, respectively) (**Fig. 7b** and **Supplementary Table 1**).

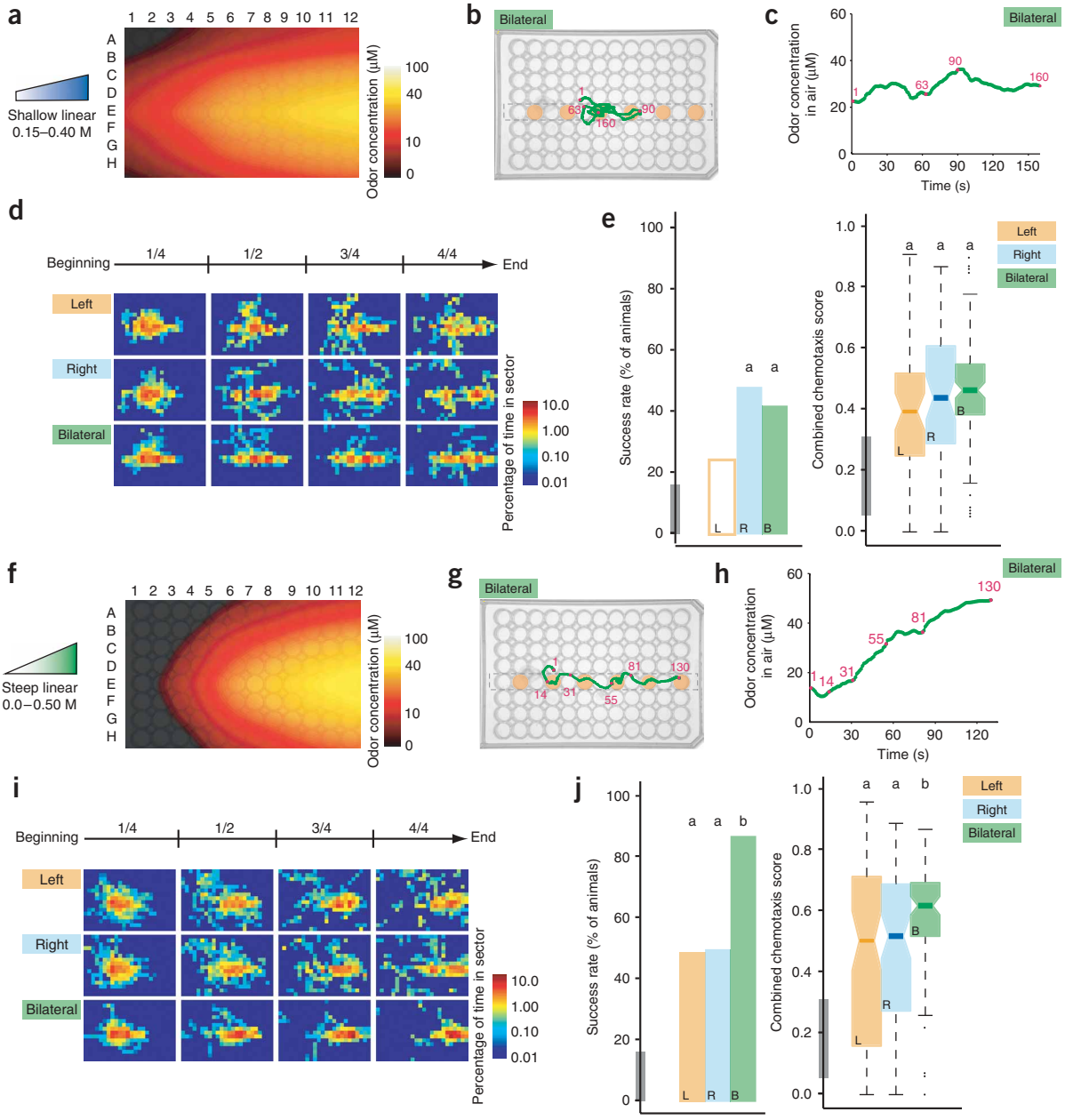

Figure 8 Bilateral sensory input enhances olfactory navigation. (**a**) Reconstructed shallow linear gradient. (**b**) Representative trajectory of a bilateral rescued animal navigating in shallow linear gradients, with four time points (s) indicated in magenta. Averaged-concentration time courses over all paths are presented in **Supplementary Figure 17** online. (**c**) Plot of odor concentration versus time of animal in **b**. (**d**) Time-sliced sector plots of unilateral left and right, and bilateral rescue trajectories tested for shallow linear gradients ($n = 80$). For a given phenotype, trajectories were subdivided into four equal time slices. Positions comprised in the same time slice were represented in one sector plot. (**e**) Statistical analysis of success rates (left) and chemotaxis score (right). Bars marked with different letters are significantly different. The gray bar on the *y* axis represents the interquartile range measured for *Or83b*$^{-/-}$ mutant tested in high-amplitude exponential gradients. (**f**) Reconstructed steep linear gradient. (**g**) Representative trajectory of a bilateral rescued animal navigating in the shallow linear gradient, with six time points (s) indicated in magenta. (**h**) Plot of odor concentration versus time of animal in (**g**). (**i**) Same as **d** for steep linear gradients (left and right, $n = 50$; bilateral, $n = 100$). (**j**) Statistical analysis of success rates (left) and chemotaxis score (right) was carried out and plotted as in **e**. In **e** and **j**, differences with *Or83b*$^{-/-}$ mutant were considered significant for corrected $P < 0.0167$. Differences between unilateral and bilateral rescues were assessed for significance using the Wilcoxon test with a Bonferroni correction (corrected $P < 0.0167$), except for the left graphs in **e** and **j** where Haber's χ^2 test was applied ($P < 0.05$ in **e**, corrected $P < 0.0167$ in **j**). Statistical analysis and data presentation are as described in **Figure 2** ($n = 80$).

Bilateral sensory input enhances olfactory navigation

Given that the small differences in the sensory threshold of unilateral and bilateral animals are unlikely to explain their considerable differences in chemotaxis performances in high-concentration gradients (**Fig. 5**), we asked whether the superior chemotaxis performance of bilateral animals could be explained by the improved signal-to-noise detection conferred by bilateral input. To test this, larval chemotaxis was carried out under more challenging conditions of linear odorant gradients with a shallow (**Fig. 8a–e**) or steep slope (**Fig. 8f–j**) along the length axis. Odors increased with an average slope of concentration as estimated from the infrared measurements of $\sim$2.0 μM cm^{-1} for shallow linear and $\sim$3.0 μM cm^{-1} for steep linear gradients (**Supplementary Fig. 16** online). For the shallow linear gradients, this resulted in a $\sim$50% reduction in the amount of odorant signal along the length axis of the gradient (**Fig. 8a**) compared with the steep linear gradient. Both gradients were designed so that the odor concentration at the start position was in the detectable range of bilateral and unilateral animals.

When faced with the challenging shallow linear gradient (**Fig. 8a**), even bilaterally rescued animals chemotaxed poorly and accumulated at the middle of the odorant line, rather than progressing to the peak zone of the gradient (**Fig. 8b–d**). Consistent with this observation, the chemotaxis scores of the unilateral and bilateral rescues were not statistically different (Kruskal-Wallis test, $P > 0.01$). Our interpretation of these results is that there is sufficient signal along the width of the plate for animals to detect the odorant line, but insufficient signal along the length of the gradient for either the unilateral or bilateral animals to navigate effectively toward the peak of the gradient.

We next tested these animals in the steep linear gradient (**Fig. 8f**). In contrast to the situation with the shallow linear gradient, bilateral animals efficiently located the center of the odorant line and progressed to the peak zone (**Fig. 8g,h**). More than 60% of bilaterally rescued animals reached the peak zone (**Fig. 8j**). Unilaterally rescued larvae chemotaxed less accurately along the odorant line, and the percentage of animals reaching the peak zone fell to $\sim$40% (**Fig. 8j**). The chemotaxis scores of unilateral animals were significantly worse than the bilateral rescue ($P < 0.0167$). We conclude that information provided by a single OSN does not permit the animal to resolve the signal from the noise along the length of the steep linear gradient, whereas the combined information carried by two OSNs is substantially above noise level.

DISCUSSION

Direct chemotaxis defines the behavioral response of a cell or a multicellular animal to chemical cues involving alignment of the direction of motion with respect to the direction of the stimulus[6]. Here, we investigated the mechanisms allowing *Drosophila* larvae to orient in an airborne odorant gradient. To study the causal relationships between stimulus conditions and behavior, we generated gradients with controlled geometries in arenas the size of a 96-well plate and developed new methods for quantifying odor concentration in gaseous phase. The paths of larvae were monitored in these arenas. The method that we developed here should be useful for creating larger controlled environments with which to study the navigation strategies of rodents and small vertebrates in free-living conditions[30,31].

By establishing a correlation between the stimulus and behavioral response, we showed that *Drosophila* larvae adopt a direct orientation strategy that is based on sequential detection of odor concentration along the path of motion. Unilateral input from a single OSN suffices for animal orientation in a gradient field, with a slight bias of performance of the right compared with the left side.

Intensity coding in the absence of combinatorial input

Chemotaxis relies on the detection of changes in chemical intensities. It has been hypothesized that odor quality and intensity are encoded by the combinatorial activation of different types of odorant receptors[32]. Accordingly, disabling part of the peripheral olfactory system should severely impair odor coding. In a previous study, we demonstrated that larvae with a bilaterally symmetric pair of *Or42a*-functional OSNs were able to respond to a large number of odorant molecules[24], and we show here that the information carried by a single pair of OSNs is sufficient to detect changes in stimulus intensity. However, we did not test the full range of concentrations and odors that the animal may encounter in its natural environment. As distinct odorant receptors may be tuned to different concentration ranges of the same stimulus[18,27], our conclusions suggest that combinatorial coding may be advantageous in expanding the sensitivity range of the overall olfactory system beyond the capacity of a single type of odorant receptor.

Larval chemotaxis relies on a direct orientation mechanism

In contrast to bacteria and *C. elegans*, which adopt an indirect orientation strategy in which turns are not preferentially aligned with the direction of the stimulus, but the length of successive steps is correlated with changes in the stimulus intensity[4,14], we showed here that *Drosophila* larvae employ a direct orientation (taxis[6]) strategy. During their ascent of odorant gradients, larvae continuously orient their turns with respect to the direction of the stimulus. The precision of the alignment between their instantaneous direction of motion and the direction of steepest concentration change improved as both the stimulus intensity and the strength of the gradient increased. To compute local odorant gradients, larvae must be able to detect differences in concentrations at different points in the gradient. This process requires either the direct comparison of odor input that is acquired by different sensors located at separate sites along the body of the animal or sequential sampling by a single set of sensors in space and time.

Both the visual and auditory systems make use of direct comparisons between left and right input to enhance sensory perception. For instance, visual depth perception necessitates input from both eyes[33]. Similarly, the localization of sound sources in space relies on the interaural time difference in the sound information that is transmitted by both ears[34]. Although bilateral sampling does not appear to be necessary for odor localization, it appears to improve odor localization in humans and other mammals[5,30]. In this study, we asked whether bilateral sampling contributes to chemotaxis performance in the *Drosophila* larva. For both *Or1a*- and *Or42a*-expressing OSNs, larvae carrying a unilateral rescue demonstrated robust chemotaxis in high exponential gradients. Our results suggest that left-right comparison is not essential for directed chemotaxis toward an odor source. On the basis of our observations, we hypothesize that larvae achieve detection of local odorant gradients by sweeping their heads laterally[23] and sampling differences in local stimulus intensity.

Odor detection is enhancement by bilateral sensory input

Although our data show that left-right comparison is not an absolute requirement for chemotaxis, there is a tangible benefit to animals with a bilateral olfactory system. Unilaterally functional larvae appeared to have more difficulty locating the center of the odorant line, meandered more along the gradient and showed an overall decrease in the accuracy of gradient sensing. Two possibilities could account for the chemotaxis impairment observed in unilateral rescues. First, impaired chemotaxis of unilateral larvae could be a trivial consequence of the marked reduction in sensory threshold as a result of a 50% reduction in input relative to a bilateral animal. Second, unilateral larvae could

show impaired chemotaxis because of a loss in signal-to-noise ratio (or overall sensitivity) compared with bilateral animals. We exclude the first possibility because the range of odor concentrations employed in our gradient is higher than the sensory threshold of both unilateral and bilateral animals. Instead, we favor the second possibility, in which sensory integration between left and right olfactory input enhances the accuracy of larval chemotaxis.

In other sensory modalities, it has been theoretically and experimentally established that signal integration, or pooling, over populations of independent and similarly tuned neurons can reduce neural noise[35]. Provided that the left and right OSNs operate in a statistically independent manner, averaging the signals coming from two bilateral OSNs could improve the signal-to-noise ratio by a factor of $\sqrt{2}$ (ref. 36). Experiments in which we modified the signal-to-noise balance in the stimulus that was presented to the animal along the plate length by changing the slope of the linear odorant gradient from shallow to steep support this signal-integration hypothesis. Taken together, our observations suggest that the pooling of signals transmitted by two bilaterally symmetric OSNs improves the quality of signal detection. We cannot exclude the possibility that signal comparison exploiting the small differences in odor concentration between left and right dorsal organs further contributes to this process.

Lateralization of the larval olfactory system

Our behavioral results suggest the existence of an unanticipated left-right asymmetry in the larval olfactory system. This may be to the result of a side-specific specification of the larval olfactory system. There are many examples of left-right asymmetry in animal behavior and central nervous function across the animal kingdom[37–41]. For instance, the human brain is highly lateralized, with different neural functions being assigned to different hemispheres. Dogs show asymmetry in the direction of tail-wagging depending on the stimulus[41]. *C. elegans* utilizes left-right asymmetry in programming the sensitivity of its peripheral olfactory neurons to enhance the coding potential and discriminative capacities of its chemosensory system[40].

For the high amplitude exponential gradients that we tested, unilateral right rescues chemotaxed significantly better than unilateral left rescues in both *Or42a*- and *Or1a*-functional animals. Because no differences were observed in the dose-response curves of the left and right rescues tested with the single odor source device, we can rule out a side-specific hypersensitivity as a result of differential levels of gene expression in the left and right neurons. We conclude that the slight right bias is an inherent feature of the larval olfactory system. It will be interesting to examine the origin of this olfactory lateralization.

Perspectives

An essential feature underlying sensory decision-making is the ability to compare one stimulus with another. If the two stimuli are presented at different times, the task is thought to involve working memory. Here, we show that larval chemotaxis is determined by the computation of local odorant gradients by active sampling of odor concentration in space and time. Our findings lead us to speculate about the existence of a fly counterpart of the working memory found in the prefrontal and parietal cortex of monkeys[42–44]. We suspect that information about odor intensities measured at different time points must be temporarily stored in working memory for the larvae to determine whether they are moving up or down an intensity gradient. On acquisition of this information, a central comparison similar to those observed in primate somatosensory delayed–match-to-sample tasks[43] must take place to direct the implementation of a turn. We do not yet know the delays that larvae can tolerate for such a comparison. This ordinal comparison mechanism does not absolutely require integration of the input transmitted by the left and right olfactory system, but we suggest that it may benefit from the enhanced signal-to-noise ratio obtained by bilateral input. Whereas long-term odor-evoked memory has received considerable attention in flies[45], it will be of great interest to identify and functionally characterize neuronal centers involved in the formation and processing of working memory that potentially underlie larval chemotaxis.

METHODS

Fly stocks. Fly stocks were maintained on conventional cornmeal-agar-molasses medium at 18 °C or 25 °C unless indicated otherwise. All animals tested behaviorally were third instar larvae. The site-specific recombinase (FLP)-out transgenic construct was injected into w^{1118} embryos by Genetic Services. The genotypes of the flies used in this study were $Or83b^{1}$ and $Or83b^{2}$ (ref. 26), and *Or1a-Gal4* and *Or42a-Gal4* (ref. 24). The hs-Flp transgene was provided by G. Struhl[46].

Generating and testing unilaterally and bilaterally rescued larvae. The Or83b FLP-out construct (*UAS>Red fluorescent protein* (*RFP*)-stop>*GFP-Orb83b*) was generated as described in the **Supplementary Methods**. Unilaterally rescued larvae were generated by crossing the parental lines *w;OrX-Gal4;hs-Flp,*$Or83b^{2}$ with *w; UAS>RFP*-stop>*GFP-Orb83b;*$Or83b^{1}$. We empirically determined that progeny of this cross contained ~25% unilaterally rescued larvae when raised at 29 °C. The proportion of bilaterally rescued larvae was only significant when 1-d-old progeny were heat shocked for 10–20 min in a 37 °C water bath. Shortly before being tested behaviorally, larvae were inspected for their pattern of GFP expression by regular fluorescence microscopy. To reduce the fraction of no-rescue larvae, individuals were sorted into three groups: no rescue, unilateral rescue and bilateral rescue. The experimenter carrying out the behavioral tests was blind to the genotype of the larvae. The anterior tips of larvae were removed after each behavioral test, fixed in a solution of 4% formaldehyde/1× phosphate-buffered saline (PBS), rinsed in PBS containing 0.1% Triton X-100 (PBS-Triton) and each sample was assessed for RFP/GFP expression by confocal microscopy without knowledge of the behavioral performance. A neuron expressing a detectable amount of GFP was considered functional irrespective of the residual presence of RFP. Heat-shock treatment did not affect the performance of unilaterally rescued larvae (**Supplementary Fig. 15**).

Odor-delivery system and FT-IR spectroscopy. All odorants were supplied at high purity by Sigma-Aldrich. We used anisole (Chemical Abstracts Service (CAS): 100-66-3), (*E*)-2-hexenal (6728-26-3), isoamyl acetate (CAS: 123-92-2) and isopropyl acetate (CAS: 108-21-4). The single and multiple–odor-source devices consist of three 96-well plate lids stacked on top of each other (see **Supplementary Fig. 1**). Either one or six of the 96 condensation rings imprinted in the top lid were filled with an odor dissolved in paraffin oil (10-µl droplets).

Odor profiles were measured at fixed positions of the plate using a FT-IR spectrometer (**Supplementary Methods**). We calculated the absolute concentration of odor in gaseous phase from the Beer-Lambert law ($A = \varepsilon \times l \times c$), where A denotes the absorbance, ε the molar extinction coefficient, l the length of the section considered and c the average concentration along this section considered. Molar extinction coefficients were determined in gaseous phase with a standard gas-flow cell (**Supplementary Fig. 3**).

Larval behavior. A single larva was introduced into the plate at position E7 (single–odor-source assay) or positions E3–E4 (multiple–odor-source device) 1 min after the odor was loaded in the top lid. Its locomotor activity was tracked with a CCD camera at a rate of 6 frames per s (6 Hz) and images were processed by Ethovision software (Noldus). Recordings in both assays lasted 3 min, unless animals contacted any walls of the plate. For the multiple source device, recordings were stopped as soon as the animals reached the highest odor concentration (row 12). Five animals were tested in approximately 15 min before the top and middle lids were replaced, consistent with the time period of gradient stability measured by FT-IR.

w^{1118} and *yw* larvae were used interchangeably as wild-type controls and showed similar chemotaxis performance (data not shown). $Or83b^{-/-}$ control genotypes were *w/w;+/+;*$Or83b^{1}/Or83b^{1}$ (**Fig. 2b**) and *w;+/+;UAS-Or83b,*

Or83b^{1}/*Or83b*^{2} (**Figs. 2e** and **4**). When tested with the multiple–odor-source device, the behavior of wild-type and *Or83b*$^{-/-}$ larvae did not differ when tested with paraffin oil only or in the absence of any odor (data not shown). Larvae with a single functional OSN were engineered by rescuing the expression of *Or83b* with *OrX-Gal4* and *UAS-Or83b* transgenes in an *Or83b*-null background as previously described[24]. The genotype of single functional OSN larvae was *w*/*w*; *OrX*-Gal4/*OrX*-Gal4; *UAS-Or83b*,*Or83b*^{1}/*Or83b*^{2}.

Data analysis. Data were analyzed in Matlab (Mathworks) with custom-written batch scripts. Sector plots were generated from trajectories without down-sampling. Sectors were defined as small squares with side lengths equal to the radius of a condensation rings. The positions of all paths recorded for the same gradient and genotype were combined and the percentage of positions per sector was computed. To enhance the contrast of the sector plot representations, logarithmic scales were used to color code the percentage of time spent in that sector.

For the single–odor-source assay, we quantified the fraction of time that a path spent in the odor zone. Two sample tests were carried out with nonparametric Wilcoxon-Mann-Whitney rank sum test (abbreviated here as Wilcoxon test). For the multiple–odor-source assay, paths were down-sampled to 1 Hz by retaining the center of gravity of clusters of six consecutive positions (**Supplementary Methods**).

For every position of the down-sampled path, we computed the local heading angle between the instantaneous direction of the path and the direction of highest concentration change obtained from the reconstructed odorant gradient (**Fig. 2d**). All angles obtained for the same experimental conditions were combined and weighted by a cosine function to form a heading distribution. Heading distributions were characterized by their means and standard errors; two-tailed *t*-tests were applied to compare pairs of heading angle samples. For the side-dependent turning-angle analysis, angular distributions were characterized by their circular means, variances and confidence intervals on the means[47].

For the multiple–odor-source, we observed that the global alignment of a trajectory with the odorant line results from two entangled trends: (i) detection of the gradient along the width of the plate and localizing the center of the odorant line, and (ii) detection of the gradient along the length of the plate and moving forward from positions 1 to 12. These two trends were quantified in a combined chemotaxis score described in the **Supplementary Methods**.

Note: Supplementary information is available on the Nature Neuroscience website.

ACKNOWLEDGMENTS

We thank K. Fishilevich, C. Ilch, S. Piccinotti, P. Rivkin, L. Salas and S. Vasquez for expert technical assistance, M. Cobb for providing the image in **Figure 5a**, and the Rockefeller University Chemical Biology Spectroscopy Research Center for access to instrumentation. This work benefited from helpful discussions with S. Benhamou, V. Jayaraman, L.C. Katz, J.D. Levine, M. Magnasco, M. Meister and D. Wolpert. We are grateful to S. Benhamou, W. Bialek, N. Buchler, M. Geffen, A.J. Hudspeth, S. Shaham and the Vosshall lab for their comments on the manuscript. This work was supported by grants from the US National Institutes of Health to L.B.V., the Ellison Medical Foundation to T.P.S., the Helen Hay Whitney Foundation to R.B., and the Belgian-American Educational Foundation and the Revson Foundation to M.L.

AUTHOR CONTRIBUTIONS

M.L. and T.H. devised and implemented the spectroscopic approach. R.B. conceived the design of the *Or83b* FLP-out construct, which was constructed together with M.L. T.P.S. provided input into the spectroscopy and supervised T.H. T.H. contributed to the conceptualization of the multiple–odor-source device, which was implemented by M.L. M.L. conceived of the project and carried out all the experiments in the paper. L.B.V. provided guidance and wrote the paper together with M.L.

Published online at http://www.nature.com/natureneuroscience
Reprints and permissions information is available online at http://npg.nature.com/reprintsandpermissions

1. Bargmann, C.I. Comparative chemosensation from receptors to ecology. *Nature* **444**, 295–301 (2006).
2. Thesen, A., Steen, J.B. & Doving, K.B. Behaviour of dogs during olfactory tracking. *J. Exp. Biol.* **180**, 247–251 (1993).
3. Wallace, D.G., Gorny, B. & Whishaw, I.Q. Rats can track odors, other rats and themselves: implications for the study of spatial behavior. *Behav. Brain Res.* **131**, 185–192 (2002).
4. Berg, H.C. *E. coli in Motion* (Springer-Verlag, New York, 2004).
5. Porter, J. *et al.* Mechanisms of scent-tracking in humans. *Nat. Neurosci.* **10**, 27–29 (2007).
6. Fraenkel, G.S. & Gunn, D.L. *The Orientation of Animals* (Dover Publications, New York, 1961).
7. Devreotes, P. & Janetopoulos, C. Eukaryotic chemotaxis: distinctions between directional sensing and polarization. *J. Biol. Chem.* **278**, 20445–20448 (2003).
8. Wadhams, G.H. & Armitage, J.P. Making sense of it all: bacterial chemotaxis. *Nat. Rev. Mol. Cell Biol.* **5**, 1024–1037 (2004).
9. Schrick, K., Garvik, B. & Hartwell, L.H. Mating in *Saccharomyces cerevisiae*: the role of the pheromone signal transduction pathway in the chemotropic response to pheromone. *Genetics* **147**, 19–32 (1997).
10. Van Haastert, P.J. & Devreotes, P.N. Chemotaxis: signalling the way forward. *Nat. Rev. Mol. Cell Biol.* **5**, 626–634 (2004).
11. Andrew, N. & Insall, R.H. Chemotaxis in shallow gradients is mediated independently of PtdIns 3-kinase by biased choices between random protrusions. *Nat. Cell Biol.* **9**, 193–200 (2007).
12. Bray, D., Levin, M.D. & Lipkow, K. The chemotactic behavior of computer-based surrogate bacteria. *Curr. Biol.* **17**, 12–19 (2007).
13. Samadani, A., Mettetal, J. & van Oudenaarden, A. Cellular asymmetry and individuality in directional sensing. *Proc. Natl. Acad. Sci. USA* **103**, 11549–11554 (2006).
14. Pierce-Shimomura, J.T., Morse, T.M. & Lockery, S.R. The fundamental role of pirouettes in *Caenorhabditis elegans* chemotaxis. *J. Neurosci.* **19**, 9557–9569 (1999).
15. Axel, R. The molecular logic of smell. *Sci. Am.* **273**, 154–159 (1995).
16. Bargmann, C.I. Genetic and cellular analysis of behavior in *C. elegans*. *Annu. Rev. Neurosci.* **16**, 47–71 (1993).
17. Uchida, N., Takahashi, Y.K., Tanifuji, M. & Mori, K. Odor maps in the mammalian olfactory bulb: domain organization and odorant structural features. *Nat. Neurosci.* **3**, 1035–1043 (2000).
18. Hallem, E.A. & Carlson, J.R. Coding of odors by a receptor repertoire. *Cell* **125**, 143–160 (2006).
19. Vickers, N.J., Christensen, T.A., Baker, T.C. & Hildebrand, J.G. Odour-plume dynamics influence the brain's olfactory code. *Nature* **410**, 466–470 (2001).
20. Gray, J.M. *et al.* Oxygen sensation and social feeding mediated by a *C. elegans* guanylate cyclase homologue. *Nature* **430**, 317–322 (2004).
21. Vetter, R.S., Sage, A.E., Justus, K.A., Carde, R.T. & Galizia, C.G. Temporal integrity of an airborne odor stimulus is greatly affected by physical aspects of the odor delivery system. *Chem. Senses* **31**, 359–369 (2006).
22. Monte, P. *et al.* Characterization of the larval olfactory response in *Drosophila* and its genetic basis. *Behav. Genet.* **19**, 267–283 (1989).
23. Cobb, M. What and how do maggots smell? *Biol.Rev.* **74**, 425–459 (1999).
24. Fishilevich, E. *et al.* Chemotaxis behavior mediated by single larval olfactory neurons in *Drosophila*. *Curr. Biol.* **15**, 2086–2096 (2005).
25. Benton, R., Sachse, S., Michnick, S.W. & Vosshall, L.B. Atypical membrane topology and heteromeric function of *Drosophila* odorant receptors *in vivo*. *PLoS Biol.* **4**, e20 (2006).
26. Larsson, M.C. *et al.* *Or83b* encodes a broadly expressed odorant receptor essential for *Drosophila* olfaction. *Neuron* **43**, 703–714 (2004).
27. Kreher, S.A., Kwon, J.Y. & Carlson, J.R. The molecular basis of odor coding in the *Drosophila* larva. *Neuron* **46**, 445–456 (2005).
28. Cobb, M., Bruneau, S. & Jallon, J.M. Genetic and developmental factors in the olfactory response of *Drosophila melanogaster* larvae to alcohols. *Proc. Biol. Soc.* **248**, 103–109 (1992).
29. Benhamou, S. & Bovet, P. Distinguishing between elementary orientation mechanisms by means of path-analysis. *Anim. Behav.* **43**, 371–377 (1992).
30. Rajan, R., Clement, J.P. & Bhalla, U.S. Rats smell in stereo. *Science* **311**, 666–670 (2006).
31. Uchida, N. & Mainen, Z.F. Speed and accuracy of olfactory discrimination in the rat. *Nat. Neurosci.* **6**, 1224–1229 (2003).
32. Hallem, E.A. & Carlson, J.R. The odor coding system of *Drosophila*. *Trends Genet.* **20**, 453–459 (2004).
33. Qian, N. Binocular disparity and the perception of depth. *Neuron* **18**, 359–368 (1997).
34. Harper, N.S. & McAlpine, D. Optimal neural population coding of an auditory spatial cue. *Nature* **430**, 682–686 (2004).
35. Parker, A.J. & Newsome, W.T. Sense and the single neuron: probing the physiology of perception. *Annu. Rev. Neurosci.* **21**, 227–277 (1998).
36. Zohary, E., Shadlen, M.N. & Newsome, W.T. Correlated neuronal discharge rate and its implications for psychophysical performance. *Nature* **370**, 140–143 (1994).
37. Letzkus, P. *et al.* Lateralization of olfaction in the honeybee *Apis mellifera*. *Curr. Biol.* **16**, 1471–1476 (2006).
38. Ehret, G. Left hemisphere advantage in the mouse brain for recognizing ultrasonic communication calls. *Nature* **325**, 249–251 (1987).
39. Vallortigara, G. & Andrew, R.J. Olfactory lateralization in the chick. *Neuropsychologia* **32**, 417–423 (1994).
40. Troemel, E.R., Sagasti, A. & Bargmann, C.I. Lateral signaling mediated by axon contact and calcium entry regulates asymmetric odorant receptor expression in *C. elegans*. *Cell* **99**, 387–398 (1999).

41. Quaranta, A., Siniscalchi, M. & Vallortigara, G. Asymmetric tail-wagging responses by dogs to different emotive stimuli. *Curr. Biol.* **17**, R199–R201 (2007).
42. Pasternak, T. & Greenlee, M.W. Working memory in primate sensory systems. *Nat. Rev. Neurosci.* **6**, 97–107 (2005).
43. Romo, R., Hernandez, A., Zainos, A., Lemus, L. & Brody, C.D. Neuronal correlates of decision-making in secondary somatosensory cortex. *Nat. Neurosci.* **5**, 1217–1225 (2002).
44. Pesaran, B., Pezaris, J.S., Sahani, M., Mitra, P.P. & Andersen, R.A. Temporal structure in neuronal activity during working memory in macaque parietal cortex. *Nat. Neurosci.* **5**, 805–811 (2002).
45. Heisenberg, M. Mushroom body memoir: from maps to models. *Nat. Rev. Neurosci.* **4**, 266–275 (2003).
46. Basler, K. & Struhl, G. Compartment boundaries and the control of *Drosophila* limb pattern by hedgehog protein. *Nature* **368**, 208–214 (1994).
47. Zar, H.J. *Biostatistical Analysis* (Prentice Hall, Upper Saddle River, NJ, 1999).